D o s s i e r

CO₂ Storage in the Struggle against Climate Change
Le stockage du CO₂ au service de la lutte contre le changement climatique

Brine/CO₂ Interfacial Properties and Effects on CO₂ Storage in Deep Saline Aquifers

C. Chalbaud[1][*][‡], M. Robin[1], J.-M. Lombard[1], H. Bertin[2] and P. Egermann[1][‡]

1 Institut français du pétrole, IFP, 1-4 avenue de Bois-Préau, 92852 Rueil Malmaison Cedex - France
2 Université de Bordeaux, TREFLE, UMR CNRS 8508, Esplanade des Arts et Métiers, 33405 Talence Cedex - France
e-mail: carlos.chalbaud@gdfsuez.com - michel.robin@ifp.fr - j-marc.lombard@ifp.fr - henri.bertin@trefle.u-bordeaux.fr -
patrick.egermann@gdfsuez.com

[*]Corresponding author
[‡]Now with GDF Suez

Résumé — **Propriétés interfaciales saumure/CO₂ et effets sur le stockage du CO₂ dans des aquifères salins profonds** — Il est admis depuis longtemps que les propriétés interfaciales (tension interfaciale, mouillabilité, capillarité et transfert de masse) régissent la distribution et le comportement des fluides au sein des milieux poreux. Par conséquent, les propriétés interfaciales entre le milieu poreux constituant le réservoir, le CO₂, la saumure et/ou le gaz du réservoir jouent un rôle important sur l'efficacité de n'importe quelle opération de stockage de CO₂. Dans le cas des aquifères salins profonds, il existe un manque de données certain en ce qui concerne les propriétés interfaciales saumure-CO₂ en conditions de stockage. Plus spécifiquement, des données expérimentales de tension interfaciale saumure-CO₂ et une meilleure compréhension du comportement de la mouillabilité en fonction des conditions thermo-dynamiques et ses effets sur l'écoulement dans le milieu poreux sont nécessaires. Dans cet article, nous présentons un jeu de données expérimentales complet de tensions interfaciales (IFT) en conditions de pression, température et salinité représentatives de celles d'un site de stockage, et une corrélation semi-analytique pour modéliser les valeurs expérimentales dont certaines ont été récemment publiées [Chalbaud C., Robin M., Lombard J.-M., Egermann P., Bertin H. (2009) Interfacial Tension Measurements and Wettability Evaluation for Geological CO₂ Storage, *Adv. Water Resour.* 32, 1, 1-109]. Cet article porte un intérêt particulier sur des tests effectués avec des échantillons de roches qui montrent un comportement mouillant du CO₂ pour des roches carbonatées de mouillabilité intermédiaire (IW) ou mouillables à l'huile (OW). Ces résultats sont cohérents avec les observations faites à l'échelle du pore en micromodèles. Ce comportement mouillant du CO₂ a un effet négatif sur la capacité de stockage d'un site donné.

Abstract — ***Brine/CO₂ Interfacial Properties and Effects on CO₂ Storage in Deep Saline Aquifers*** — *It has been long recognized that interfacial interactions (interfacial tension, wettability, capillarity and interfacial mass transfer) govern fluid distribution and behaviour in porous media. Therefore the interfacial interactions between CO₂, brine and reservoir oil and/or gas have an important influence on the effectiveness of any CO₂ storage operation. There is a lack of experimental data related to interfacial properties for all the geological storage options (oil & gas reservoirs, coalbeds, deep saline aquifers). In the case of deep saline aquifers, there is a gap in data and knowledge of brine-CO₂ interfacial properties at storage conditions. More specifically, experimental interfacial tension values and experimental tests in porous media are necessary to better understand the wettability evolution as a function of thermodynamic conditions and it's effects on fluid flow in the porous media. In this paper, a complete set*

of experimental values of brine-CO_2 Interfaciale Tension (IFT) at pressure, temperature and salt concentration conditions representative of those of a CO_2 storage operation. A correlation is derived from experimental data published in a companion paper [Chalbaud C., Robin M., Lombard J.-M., Egermann P., Bertin H. (2009) Interfacial Tension Measurements and Wettability Evaluation for Geological CO_2 Storage, Adv. Water Resour. 32, 1, 1-109] to model IFT values. This paper pays particular attention to coreflooding experiments showing that the CO_2 partially wets the surface in a Intermediate-Wet (IW) or Oil-Wet (OW) limestone rock. This wetting behavior of CO_2 is coherent with observations at the pore scale in glass micromodels and presents a negative impact on the storage capacity of a given site.

DEFINITIONS, ACRONYMS, ABBREVIATIONS

C	Constant related to the Parachor number
k_r	Relative permeability
m	Molal concentration (n°moles/kg of solvent)
M	Molar mass
P	Parachor number
P_c^{th}	Capillary pressure threshold
P_{CO_2}	Pressure in the CO_2 phase
P_w	Pressure in the aqueous phase
R	Size of the largest connected pore throat in the caprock
T	Temperature
x	Molar fraction of component i in the liquid phase
x_{NaCl}	Molal concentration in NaCl
y	Molar fraction of component i in the vapor phase

ADSA	Axi-symmetric Drop Shape Analysis
Hg	Mercury
IFT	Interfaciale Tension
IEA	International Energy Agency
IW	Intermediate Wet
NMR	Nuclear Magnetic Resonance
OW	Oil Wet
PNM	Pore Network Modeling
ppm	Parts per million
WW	Water Wet

α	Exponent of the corrective factor P/M
β	Correlation coefficient for the reduced temperature
γ	Interfacial tension
γ_0	Reference interfacial tension
γ_{w,CO_2}	Water-CO_2 interfacial tension
γ_{b,CO_2}	Brine-CO_2 interfacial tension
$\gamma_{Wplateau}$	Water-CO_2 interfacial tension plateau value
δ	Scaling exponent for the interfacial tension
$\delta\gamma$	Increase of the interfacial tension due to salt.
$\Delta\rho$	Density difference
φ	Scaling exponent for the density difference
λ	Correlation coefficient for the salt concentration
η	Correlation coefficient for density difference
ρ	Phase density
θ	Contact angle

SUBSCRIPTS

c	Critical point
i	Constituent index
l	Liquid
r	Reduced, current to critical state ratio
v	Vapour
0	Reference

INTRODUCTION

Large-scale subsurface storage of anthropogenic carbon dioxide is considered as a potential technology for greatly stabilizing greenhouse gas concentration in the atmosphere [1]. At least three options exist for geological storage of CO_2 [2]: oil and gas reservoirs, deep saline aquifers and unmineable coal beds. Because of its expertise and knowledge of many geological sites considered as prospects for CO_2 storage, the oil industry is usually uniquely positioned to sequester CO_2, no matter the source. Successful CO_2 sequestration in deep saline aquifers and different types of hydrocarbon reservoirs is largely governed by the fluid-fluid and fluid-rock interfacial interactions. These interactions are represented by the Laplace equation *(see Eq. 1)*, where the key parameters to take into account are the interfacial tension and the wettability. Therefore, the quality of the data related to these properties is particularly important in CO_2 storage modeling. On the one hand these properties highly influence the flow process, and on the other hand they control the capillary-sealing efficiency:

$$P_c = P_{CO_2} - P_{Brine} = \frac{2 \cdot \gamma_{b,CO_2} \cdot \cos\theta}{R} \tag{1}$$

where P_c is the capillary pressure, γ_{b,CO_2} is the brine-CO_2 interfacial tension, R is the largest connected pore throat and θ is the contact angle, which is related to reservoir wettability.

This paper deals with γ_{b,CO_2} and wettability at CO_2 storage conditions. For interfacial tension, experimental data of pure water-CO_2 system at reservoir conditions, γ_{w,CO_2} have been reported by several authors since 1957 [3-6]. Nevertheless, there are some concerns with the use of these data [6], related to the thermodynamic equilibrium, the image analysis

method which was used, and the non consideration of the dissolved CO_2 effect on the water phase density [7]. At the same time, efforts to estimate γ_{w,CO_2} from molecular dynamics computer simulations [8, 9] or theoretical models [10-12] have not lead to satisfactory results. To our knowledge, there is no complete set of experimental data concerning the brine-CO_2 system (at high pressures, high temperatures and different salt concentrations), which could be used to estimate γ_{b,CO_2} under representative storage conditions.

To our knowledge, as far as wettability is concerned, the only significant contributions to gather data and knowledge, have been focused on capillary seal efficiency of the caprock. Chiquet *et al*. [12] measured contact angle between CO_2 and brine, on both mica and quartz surfaces. According to the authors, there is change in the contact angle while increasing the pressure; this indicates a passage from a strongly water-wet media to an intermediate-wet media. Chiquet [13, 14] explanations are based on the DLVO theory (disjoining pressure). Chiquet points out a strong change in electrostatic forces while increasing the pressure. This change is a consequence of pH reduction, due to the dissolution of CO_2 in the aqueous phase. Such wettability alteration is detrimental to CO_2 geological storage because it induces lower breakthrough pressures across the caprock *(see Eq. 2)*. To our knowledge, no other analogous work can be found in the literature which study fluid flows and phase distributions in silica or carbonate rocks for different wettability scenarios.

$$P_c^{th} = P_{CO_2} - P_{brine} = \frac{2\gamma_{b,CO_2}\cos\theta}{R} \qquad (2)$$

where P_c^{th} is the threshold capillary pressure in the caprock saturated with brine, and R the largest connected pore throat in the caprock.

1 APPROACH

Three different scales are investigated in this paper: the interface, the pore scale (Poiseuille) and the rock scale (Darcy). For the Interfaciale Tension (IFT), the Axi-symmetric Drop Shape Analysis technique (ADSA) was used, in the case of a rising drop. These measurements have been performed for pressures ranging from 45 to 255 bars, temperatures from 27 to 100°C and NaCl concentrations (salinity) from 5000 to 150 000 ppm. A correlation was then developed on the basis of the Parachor model, the salt effect and a regression fit of more than one hundred IFT experimental values. For the wettability, glass micromodels have been used to study qualitatively the fluid distribution in the case of different wettabilities and thermodynamic conditions. Next, in order to obtain quantitative data, CO_2 and N_2 core flooding tests were performed in a carbonate core sample. During these tests local saturation measurements have been carried out and the heterogeneous approach [17] was used for the numerical interpretation. P_c curves for different wettability scenarios have been estimated.

2 BRINE-CO₂ INTERFACIAL TENSION

2.1 Experimental Section

For a given salt concentration and a given temperature, an average of ten $\gamma_{b,CO2}$ values were measured. Thermodynamic conditions ranged from 45 bars up to 255 bars; three temperatures 27, 71 and 100°C, and four salinities (5000; 50 000; 100 000 and 150 000 ppm) were investigated. The density values of brine solutions were calculated from Søreide and Whitson [16] and Rowe and Chou [17]. This calculation takes into account the effect of dissolved CO_2 and NaCl. The CO_2 density was considered as equal to that of pure CO_2 according to King *et al*. [18].

2.2 Experimental Equipment

The experimental set-up presented in Figure 1 is designed to work under representative reservoir conditions (up to 260 bars and 120°C). It allows measurements of interfacial tension for two phase systems using the rising (or pendant) drop method.

This device consists of three items: the high pressure visualization cell, the fluid circuit and feeding system, and the imaging system. A CO_2 cap is maintained at the ceiling of the visualization cell in order to improve the thermodynamic equilibrium. For the same reason, fluids are pre saturated under the same conditions as the measurements. This means that, in the CO_2 cell CO_2 is equilibrated with brine and in the brine cell brine is in contact with CO_2). The term "pre saturate" is used instead of "saturate" because experiments showed that using this method does not lead to a perfect stabilization and to a complete saturation of both phases [6]. The imaging system consists of a linear arrangement of a light source, a glass diffuser, the rising drop and the digital camera.
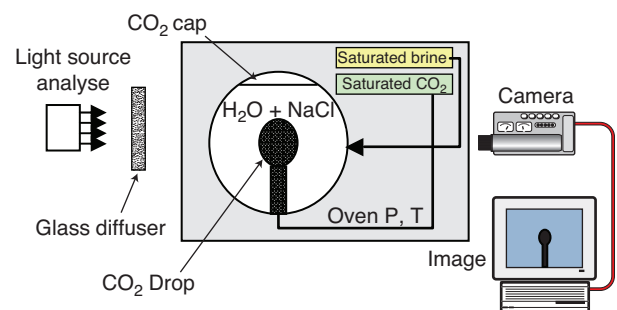

Figure 1

Experimental set-up.

Drop-shape techniques have been widely used and are among the most accurate methods. The Axi-Symmetric Drop Shape Analysis (ADSA) was selected for this study. ADSA acquires images of a drop and extracts the experimental profile of this drop, using edge detection techniques. Details of the ADSA methodology can be found elsewhere [19].

2.3 Experimental Procedure

CO_2 drops are generated at the tip of a glass capillary tube (1.5 mm o.d) in the visualization cell, which has been previously filled with the brine solution. A CO_2 cap is placed at the ceiling of this cell to maintain a good CO_2 saturation of the brine solution within the cell. The capillary tube is also used as an internal metric standard to determine the exact drop size. A range of pressures between 45 and 255 bars was investigated along each isotherm, using a compression process. For each pressure step, the IFT was obtained taking the average of at least 5 measured values.

As the equilibrium of the system is of primary importance to the accuracy of the measurements, once the drop is generated and enlarged at the tip of the capillary, it was maintained in the cell during several minutes. Measurements were taken over time during this period as shown in Figure 2. The equilibrium IFT is a static value that was reached almost 8-15 min after the drop was generated, depending on the thermodynamic conditions. The period during which IFT decreases corresponds to the dissolution of CO_2 in brine and vice versa. If CO_2 is not pre saturated before the drop formation and if the CO_2 ceiling is not present in the visualization cell, static IFT values would be more difficult to achieve. The evolution of the IFT presented in Figure 2 is the consequence of using the saturated aqueous phase density values
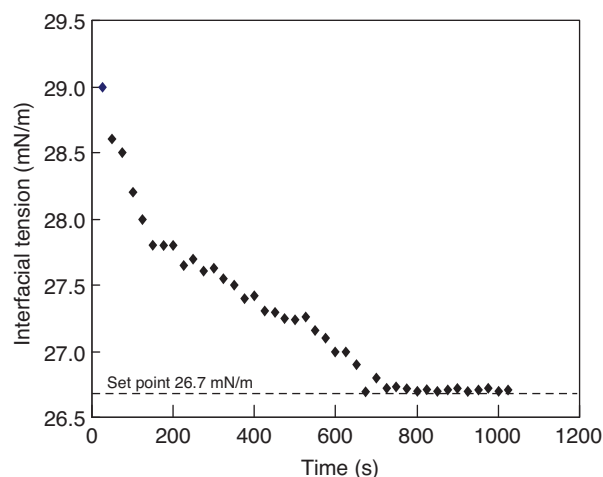
(equilibrium not reached), instead of the instantaneous ones. As densities cannot be measured in the viewing cell, the only possible approach was effectively to consider this saturated aqueous phase density for all the points and to wait until a constant value of IFT was reached.

2.4 Results and Discussion

2.4.1 Brine/CO_2 IFT *vs* Pressure and Temperature

All results are presented in terms of NaCl molal concentration, in order to allow comparison of the linear relationship between the increase in the IFT and the molal concentration of salt observed by previous authors mentioned in the introduction. The maximum standard deviation of the presented experimental data is close to 3.5%. A complete description of these results will be found in Chalbaud *et al.* [20] γ_{b,CO_2} isotherms were obtained at 27, 71 and 100°C. Figure 3a shows isotherms at 27°C. The evolution of γ_{b,CO_2} with pressure and temperature is similar to the one reported by other authors for γ_{w,CO_2}, under similar conditions [3-6]: at low pressures γ_{b,CO_2} decreases with pressure; this decrease is more pronounced at low temperature. At high pressures a plateau value of γ_{b,CO_2} is reached for all NaCl concentrations investigated. At 27°C this plateau is reached at 80 bars, while at 71°C, it is reached at 150 bars. At 100°C it is not possible to claim that a plateau has been reached. It is interesting to note that the pressure at which this plateau is reached does not depend on the NaCl concentration neither at 27°C nor at 71°C. Nevertheless, the value of γ_{b,CO_2} at the plateau does depend on the salt concentration. At these temperatures the γ_{b,CO_2} value is the same once the plateau has been reached. It is of approximately 26 mN/m for 5000 ppm of NaCl. At highest temperatures (100°C), the minimal γ_{b,CO_2} is also close to 26 mN/m for 5000 ppm. We call this value $\gamma_{W plateau}$, where the W subscript refers to a very low salinity brine or to pure water. For a similar range of temperatures and pressures, several authors [3, 6] have already reported the presence of a plateau in the IFT of pure water-CO_2.

Figure 3a presents the IFT of pure water-CO_2 and those of brine-CO_2 at different salt concentrations at 27°C. It can be seen from this figure that the difference between the measured IFT values for pure water and the lowest salinity brine (5000 or 0.085 m) is negligible. The results at 0.085 m NaCl can be considered as analogous to those of pure water. For such a low NaCl concentration a negligible effect of salt has already been reported for pressures up to 60 bars [21].

Figure 3b presents the same experimental results in a different manner. This figure presents an iso-salt concentration at 0.87 m NaCl. Similar results have been obtained for different values of salt concentration. At high pressures, the γ_{b,CO_2} reaches a constant value that does not depend neither on the pressure nor on the temperature. At high pressures, CO_2 becomes nearly incompressible (constant $\Delta\rho$). At lower
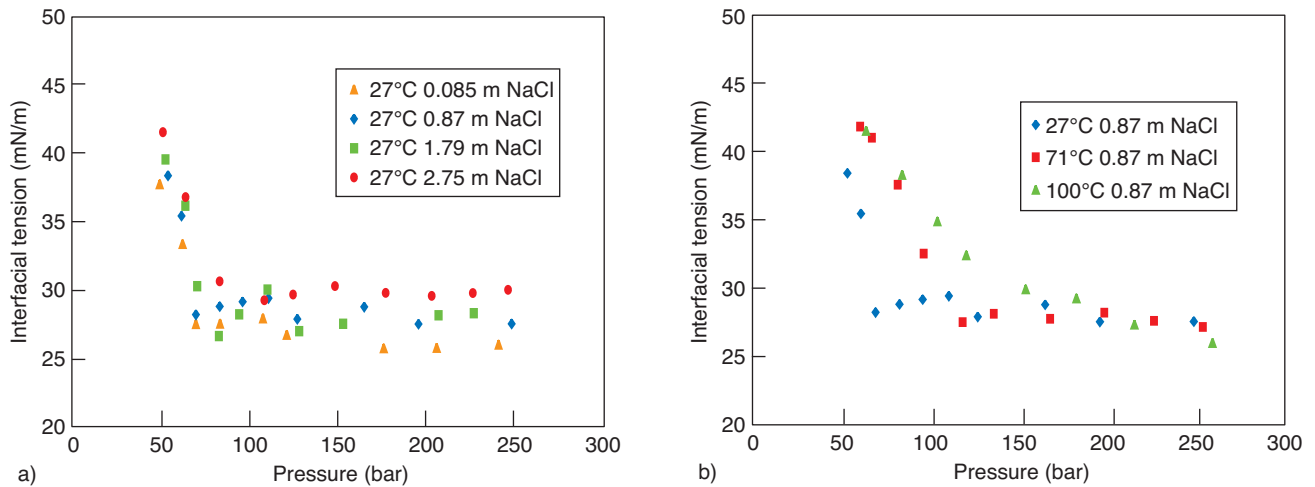

Figure 2

Change of the IFT over time. P = 120 bars, T = 27°C and [NaCl] = 5000 ppm.

Figure 3

a) IFT as a function of pressure for different NaCl molal concentration at $T = 27°C$, b) IFT as a function of pressure for different temperatures and NaCl concentration 0.87 m (50 000 ppm).
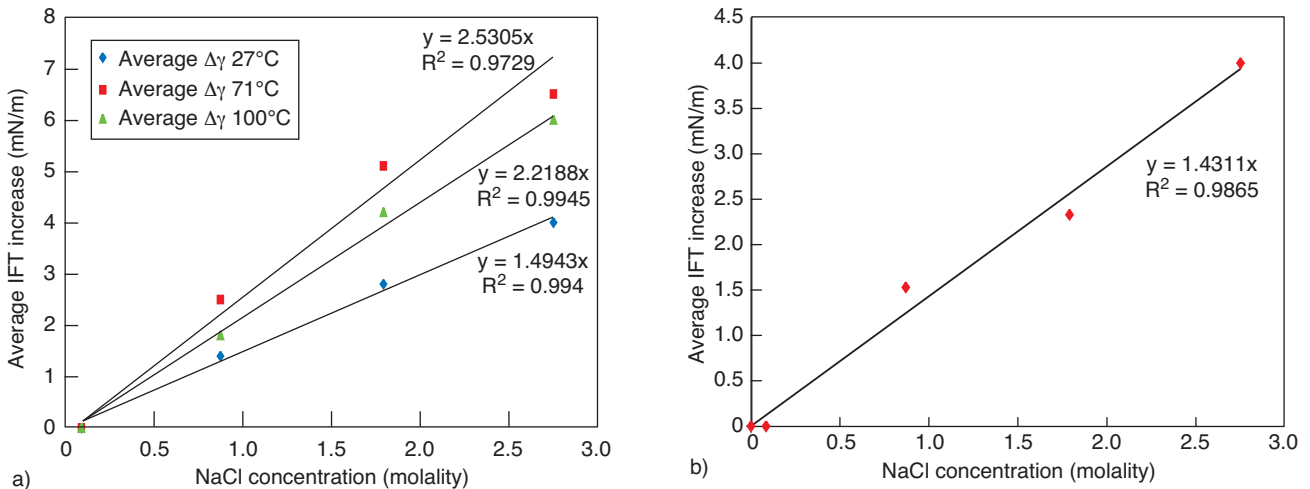

Figure 4

Average increase of the IFT as a function of the NaCl molality for different temperatures, a) before reaching a plateau and b) after the IFT plateau.

temperatures this incompressibility is reached for a lower pressure. A similar evolution of CO_2 solubility in water and brine with pressure has been reported [22-24] (additional CO_2 solubility in brine from an increment in pressure strongly decreases at higher pressures).

This clearly shows that there is an important reduction of phase and solubility effects on the interfacial tension that could explain the existence of plateau in the γ_{b,CO_2} above a given pressure. This value therefore depends only on the temperature. These results point out a possible extrapolation of γ_{b,CO_2} for higher pressures, and establish a value of 26 mN/m ($\gamma_{Wplateau}$) for pure water or very low salinities (and other values according only on the salt concentration).

The applicability of this suggestion at temperatures near or above 100°C would need additional γ_{b,CO_2} experimental values for pressures above 300 bars.

2.4.2 γ_{b,CO_2} vs Salt Concentration

Similarly to previous works [21, 25], a linear relationship between the increase of brine-CO_2 interfacial tension and molal salt concentration was found. This increase becomes more important at higher temperatures, as shown in Figure 4a. Once the plateau is reached the influence of temperature on the IFT becomes negligible. Therefore it is possible to establish an IFT increase independent of the temperature once the

plateau is achieved *(Fig. 4b)*. Before reaching the plateau at 27°C this linear relationship is as follows:

$$\delta\gamma = 1.49m \qquad (3)$$

where $\delta\gamma$ represents the increases of the IFT and m represents the molal concentration of salt. At $T = 71°C$ and $T = 100°C$ the slopes $\delta\gamma/m$ of the linear relation before reaching the plateau are higher *(see Fig. 4)*. After reaching the plateau we found a unique slope value (independent of the temperature) of 1.43. According to Argaud [25] IFT increase is given by a slope $\delta\gamma/m$ of 1.63 for a water-air system at ambient conditions. In the case of NaCl, this relation is almost constant over a large range of molalities. Similar relationships exist for other chlorides at ambient conditions [25]. For KCl, MgCl$_2$ and CaCl$_2$ this increase is not linear at high values of molalities (>1.0m). Nevertheless, in most of the cases the concentration of these salts in reservoir brines is in the range of molalities inside which linear relations has been reported. There is no available data to evaluate the interfacial tension increase for a system which contains different salts, for example to know whether this increase would be additive or not.

Massoudi and King [21] have found $\gamma_{b,CO2}$ values at 25°C for the brine-CO$_2$ system that indicated a linear relationship between the $\gamma_{b,CO2}$ and the molal concentration of NaCl (up to 5m) for pressures up to 60 bars. The $\delta\gamma/m$ slope was near to 1.58 instead of 1.49 as presented in Equation (3). They also found a very slight (negligible according to the authors) decrease of this coefficient with pressure.

The evolution of the interfacial tension increase with molal concentration of NaCl in water is analogous to that reported by Massoudi and King [20] and those summarized by Argaud [25]. At 27°C, and after reaching the plateau, the value of the coefficient obtained for the linear relationship is very close to those reported by the above authors. These results do not support a proportional relation of the IFT increase with the Kelvin temperature suggested by Aveyard and Saleem [26], and Johansson and Eriksson [27]. In fact the difference in the IFT increase we observed between 71°C and 100°C is within the standard deviation of our results.

2.4.3 Possible Implications on CO$_2$ Storage

The available data existing in literature, which could be used by reservoir engineers to estimate IFT of water-CO$_2$ systems, do not take into account the effect of CO$_2$ dissolution on the aqueous phase density. At high pressure and low temperature, this effect becomes more important, because the density difference between the brine and the CO$_2$ is minimal. For example: at 27°C and 240 bars, the density difference is 14% lower if the dissolution of the CO$_2$ into the brine phase is not taken into account. Recently, Chiquet *et al.* [28] showed that under a pressure of 450 bars, this difference can be up to 70%. Due to the fact that density difference enters linearly in the IFT calculation, this could explain why at high pressures (once the plateau has been reached), there is a difference in

$\gamma_{w,CO2}$ reported values, between low and high temperatures [6]. This indicates that available $\gamma_{w,CO2}$ data could be underestimated, especially at low temperatures. Chiquet *et al.* [28] have studied the interfacial tension of brine-CO$_2$ systems, for very low salinity, for high pressures (up to 450 bars), and a similar range of temperatures. They report a similar IFT plateau for a temperature lower than 100°C. This means that the IFT values reported in this paper for pressures up to 255 bars could be extrapolated up to 450 bars. Concerning the implications of salt effects, we observed that for salt (NaCl) concentrations above 30 000 ppm, the IFT increase is higher than the standard deviation; therefore it should not be neglected.

Additionally, if reported effects of CaCl$_2$ or MgCl$_2$ [29], both present in carbonate reservoirs, on surface tension, are extrapolated to high pressure and a wide range of temperatures, the increase of IFT due to their presence in the brine would be near the double of that of NaCl at storage conditions. This means that for pressures over 150 bars and temperatures between 27 and 71°C, the increase would be close to 8 mN/m for CaCl$_2$ or MgCl$_2$, instead of 4 mN/m measured for 150 000 ppm of NaCl. This increase is as high as 30% of the $\gamma_{w,CO2}$ value. Therefore, the estimation of the $\gamma_{b,CO2}$ at storage condition, without taking into account the dissolved CO$_2$ in the aqueous phase nor the effect of salts, is strongly underestimated.

If $\gamma_{b,CO2}$ is underestimated, the capillary pressure threshold (P_c^{th}) calculated from Equation (2), which determines the CO$_2$ breakthrough in the cap rock and the height of CO$_2$ column stored, is also underestimated; this leads to an underestimation of the storage capacity of the reservoir.

In the case of CO$_2$ storage in a deep saline aquifer, $\gamma_{b,CO2}$ governs fluid distribution in the porous media and is a key parameter in reservoir simulations to estimate the water displacement by a CO$_2$ injection. For a given height of stored CO$_2$, the underestimation of $\gamma_{b,CO2}$ leads to an overestimation of the displacement efficiency of a CO$_2$ flooding in a deep saline aquifer; hence, it increases the amount of displaced brine and could erroneously increase the available reservoir storage volume for CO$_2$.

Figure 5 shows the cumulative brine production for CO$_2$ flooding in a carbonate core saturated with brine, at two different salinities (from Egermann *et al.* [30]). These experiments were carried out at the same pressure and temperature, $P = 100$ bars and $T = 80°C$, and two different salinities: 5000 ppm and 150 000 ppm. This figure shows that when the cumulative brine production has reached a constant value, this value is 13% higher for the lowest brine salinity, hence the available reservoir storage volume for CO$_2$ is 13% higher. According to Egermann *et al.* [30], this difference is due to the difference in the interfacial tension: it is possible to perform a satisfactory history match from reservoir simulations of both experiments, with the same k_r and P_c curves, if the P_c curves are corrected using $\gamma_{b,CO2}$ values which take into account the salinity.
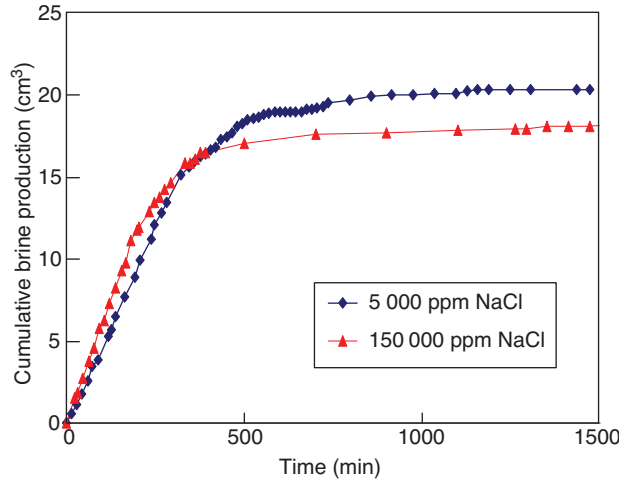
Figure 5

CO_2 flooding in a carbonate core saturated with NaCl brine at two different salt concentrations. $P = 100$ bars and $T = 80°C$.

2.5 IFT Modeling

For water-pure hydrocarbon systems, Firoozabadi and Ramey [31] presented some examples using the Parachor model for multicomponents systems [32] *(see Eq. 4)*. According to the authors this equation fails to predict the IFT for several water-hydrocarbon systems.

$$\gamma = \left[\sum_{i=1}^{n} P_i \left(x_i \frac{\rho_l}{M_l} - y_i \frac{\rho_v}{M_v} \right) \right]^4 \tag{4}$$

Firoozabadi and Ramey [31] proposed a correlation analogous to the Parachor model because it correlates the IFT to the density difference, with an exponent 4 (critical scaling exponent). Two correlation parameters have been used by Firoozabadi and Ramey [31]: the density difference between the hydrocarbon phase and the water phase and the reduced temperature. In this correlation the *y*-axis is:

$$\left(\frac{\gamma^{0.25}}{\Delta\rho} \right) * T_r^{0.3125} \tag{5}$$

and the *x*-axis is the density difference, $\Delta\rho$. Although Firoozabadi and Ramey [31] showed that when using this correlation, the interfacial tension of several water-hydrocarbon systems at different thermodynamic conditions, is represented by a single curve; however it is not the case for some gases such as n-propane, ethylene and CO_2. To develop this correlation the effect of gas dissolved in water or water dissolved in gas is not taken into account. This correlation originates from an assumed similarity between the water-liquid

hydrocarbon IFT and the surface tension of the hydrocarbon at the same thermodynamic conditions [23]. Subsequently, Argaud [25] proposed to use the Parachor number to molar mass ratio of the hydrocarbon and an exponent, α, as a corrective factor to the correlation proposed by Firoozabadi and Ramey [31] as follows:

$$\left[\frac{\gamma^{\frac{1}{4}} * Tr^{0.3125}}{\left[\Delta\rho * \left(\frac{P}{M} \right)^\alpha \right]} \right] \tag{6}$$

This corrective factor is based on the McLeod equation for pure compounds [33] reviewed by Fowler [34]:

$$\gamma^{\frac{1}{4}} = \frac{P}{M} \Delta\rho_{lv} \tag{7}$$

where $\Delta\rho_{lv}$ is the density difference between the liquid and vapour phases of a pure hydrocarbon.

From Equation (6), Argaud [25] obtained a better fit to available IFT data for other gases compared with Firoozabadi and Ramey [31]. The idea is that $\Delta\rho$ is not the only parameter to be used for IFT prediction and additional information has to be sought from the chemical structure of the hydrocarbon through its hydrocarbon Parachor number.

The experimental results of this study indicate that γ_{b,CO_2} is strongly correlated with $\Delta\rho$ *(see Fig. 6)*. The density difference takes into account the combined effects of pressure and temperature, and part of the salt effect as well. Nevertheless, $\Delta\rho$ is not enough to predict the γ_{b,CO_2}. Figure 7 show that for the same $\Delta\rho$, different IFT can be obtained. This is mainly due to the salt effect. The observed existence of a plateau in the γ_{b,CO_2} is strongly related with the density difference. For density differences below 0.6 g/cm³, a stabilization in the has been observed, and the only parameter that affects the γ_{b,CO_2} is the salt concentration.

In order to model the interfacial tension, it is necessary to separate its variation with the density difference in two parts *(see Fig. 7)*. The first part (high $\Delta\rho$) could be correlated with equations similar to the Parachor model for pure compounds *(Eq. 7)*. The second part (low $\Delta\rho$), which corresponds to the plateau, has to be correlated using the γ_{w,CO_2}, once the plateau is reached ($\gamma_{Wplateau}$), and a linear relationship, to match the increase due to the presence of dissolved salts. Then, γ_{b,CO_2} can be explicitly described as:

$$\gamma_{b,CO_2} = \gamma_{Wplateau} + \lambda * x_{NaCl} + \left[\frac{P}{M} (\Delta\rho) \right]^\eta * T_r^\beta \tag{8}$$

where λ, β, θ are regression coefficients obtained from a least-squares fit of our results. The values of these coefficients are presented in Table 1. P, M and $\gamma_{Wplateau}$ are
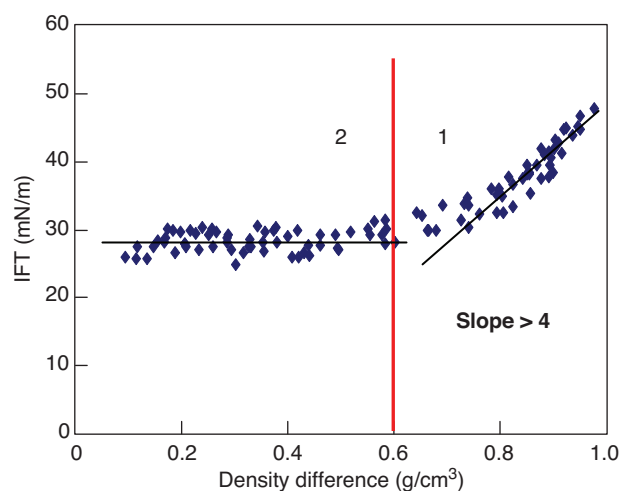
Figure 6

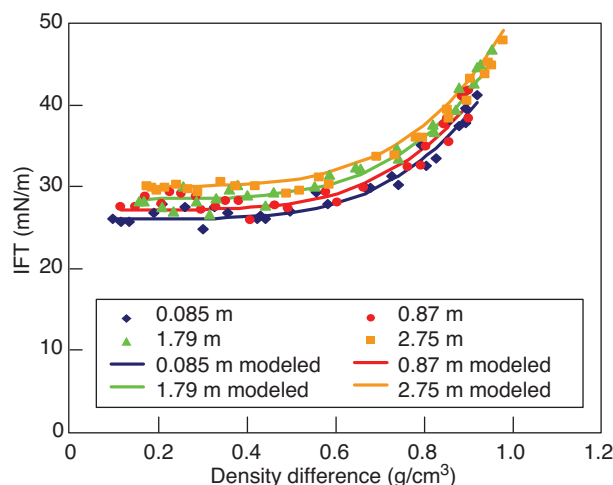Variation of the interfacial tension of brine-CO_2 systems with density difference.

Figure 7

Experimental and modeled IFT values.

constant values presented in Table 2. *P* and *M* are respectively the Parachor number and the molar mass of CO_2. As "α" exponent was always close to 1 it was decided not to use the "α" exponent or the *P/M* factor *(Eq. 6)* and a good regression fit of the results was obtained.

<div align="center">

TABLE 1

Coefficients of the regression fit *(Eq. 8)*

λ	1.2550
η	4.7180
β	1.0243

TABLE 2

Constants values used in Equation (8)

P (CO_2 Parachor number)	82
M (g/mol)	44.01
$\gamma_{Wplateau}$(mN/m)	26

</div>

It can be considered as arbitrary not to use the density difference with an exponent 4; but as Schechter and Guo [35] explained in a comprehensive review of the Parachor model and its use in IFT prediction of fluids, the IFT of several systems deviates from a slope of 4 to higher values. This behavior is attributed to molecules which rapidly adsorb at the interface. In this case the IFT would be significantly reduced although the density difference between the bulk phases would change very little *(Fig. 7, part 1)*.

In the proposed correlation, T_r was only used as a corrective factor because at lower pressures *(Fig. 6, part 1)*, the IFT increase due to the presence of dissolved salts

becomes higher with temperature. Hence, the use of a constant parameter related to salts effects (λ, *Tab. 1*) is compensated with the use of the T_r.

The correlation proposed in Equation (7) takes into account pressure, temperature and salt effects, as well as the influence of the chemical structure of the CO_2. Figure 8 shows the modeled $\gamma_{b,CO2}$ using Equation (8) *vs* the experimental data, under the same conditions. From the regression fit of our experimental results, it is possible to predict the $\gamma_{b,CO2}$, using only three regression coefficients with a mean deviation of 2.5% and more than 96% of the calculated values below a deviation of 6% from the experimental values.

3 WETTABILITY

3.1 Visualization Experiments

In order to study the fluid flow and distribution in the porous media for different wettability conditions, glass micromodels were used. The tests were conducted with water-wet, intermediate-wet and oil-wet micromodels. The micromodels were initially fully saturated with water and then flooded with CO_2 under different thermodynamic conditions.

3.2 Experimental Facilities

Figure 8 shows the experimental set-up. The micromodel can be operated at pressures up to 100 bars and temperatures up to 60°C.

Transparent glass micromodels are made of two glass plates. On one of them, a two dimensional network of pores has been etched. The transparent nature of the micromodel
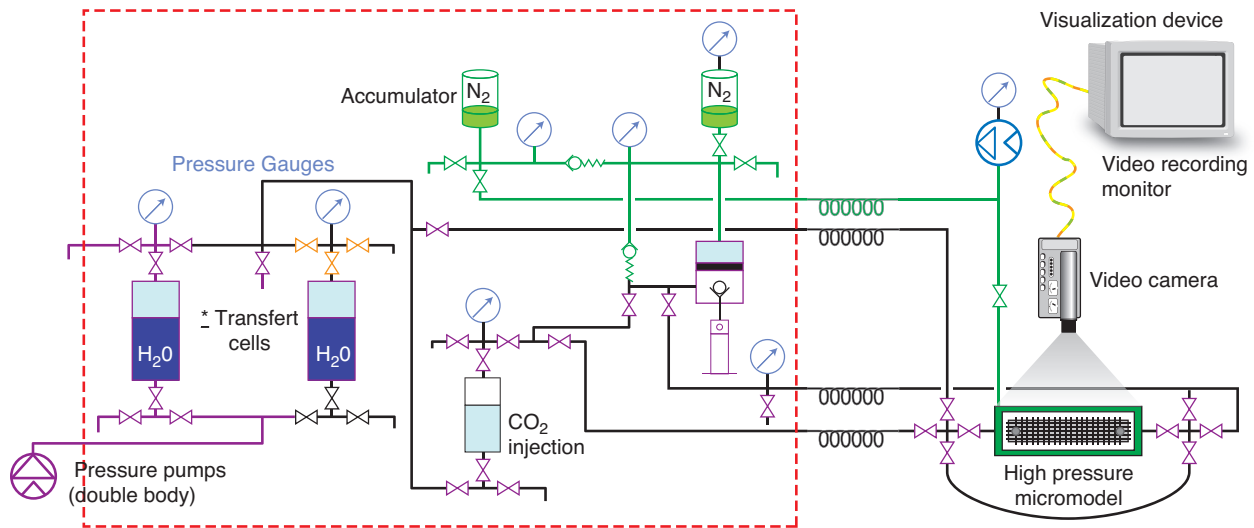
Figure 8

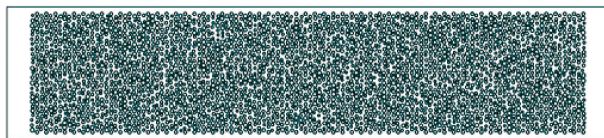Experimental set-up for micromodel visualization.

Figure 9

2-D pore network.

allows the pore-scale multiphase displacement to be observed and recorded. For this study, the micromodels consist of a porous area of 6.5 cm × 1.25 cm. For the used heterogeneous network the solid surface is represented by round grains, and the fluid path by the space between these grains. The design corresponds to a random grain size and location *(Fig. 10)*.

Glass micromodels are originally water-wet. In order to obtain an intermediate wettability the entire porous medium has been aged with a heavy crude oil. In order to obtain an oil-wet medium we treated the surface with a silane. Details of this treatment can be found elsewhere [36].

3.3 Experimental Procedure

The micromodel was initially saturated with distilled water. Then CO_2 was injected at a low rate. The injection rate at all stages was 1cc/h (0.5 PV/h). Experiments were video recorded until the fluid distribution in the porous media was static. At the end of each experiment the micromodel was flushed with distilled water until reaching a 100% water saturation. Then thermodynamic conditions of the set-up were changed for the next experiment.

3.4 Results and Discussion

Table 3 presents the thermodynamic conditions of all experiments carried out in this study. These conditions have been chosen in order to be able to visualize the fluid distribution for all the CO_2 physical states: gaseous, liquid and supercritical. A more detailed description of our results, including all images, could be found elsewhere [37].

TABLE 3

Experimental conditions

Wettability	Pressure (bar)	Temperature (°C)	CO₂ Phase
WW	57.9	20.0	Gas
WW	105.4	60.0	Supercritical
WW	100.0	23.0	Liquid
IW	60.0	25.0	Gas
IW	100.0	60.0	Supercritical
IW	100.0	25.0	Liquid
OW	51.3	19.0	Gas
OW	100.0	60.0	Supercritical
OW	100.0	23.0	Liquid

3.4.1 Water-Wet

In the water-wet experiment we observed that the water is always the wetting fluid. This looks obvious from the shape of the interfaces; it is also possible to draw this conclusion from the existence of very thin water films around the grains *(see Fig. 10)*. Chiquet *et al.* [13], reported water-CO₂ contact angle values on silica surfaces (quartz and mica). By means of contact angle measurements, the authors showed that the
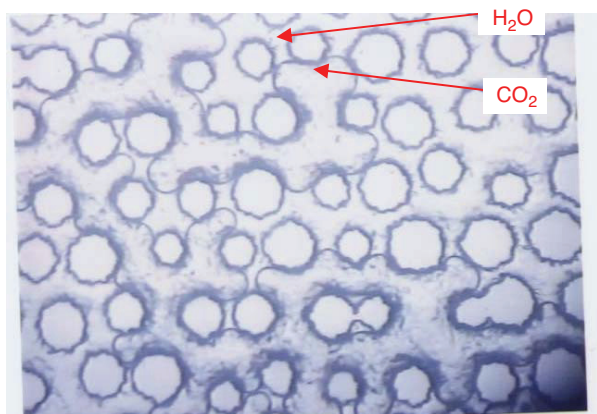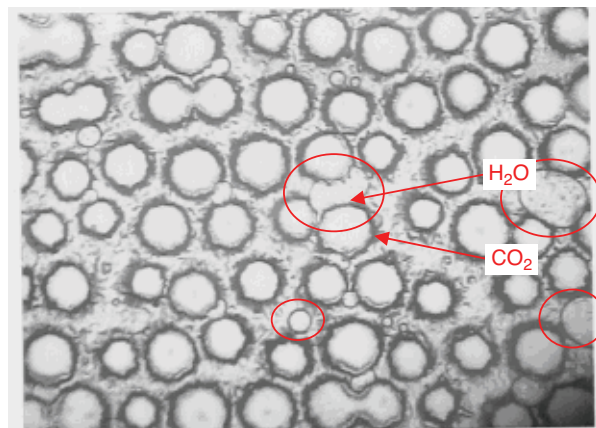
Figure 10

WW micromodel. $P = 100$ bars, $T = 23°C$.

Figure 11

IW micromodel. $P = 100$ bars, $T = 25°C$.

water-wettability of minerals representative of shales, such as mica and quartz, is significantly altered by the presence of CO_2, under pressures representative of geological storage conditions (100 bars). Therefore, those minerals, known to be strongly water-wet in the presence of oil, turn out to be intermediate-wet in the presence of dense CO_2. The authors explain this change in wettability using the DLVO theory [38]. According to this theory, the stability of the water films on the solid surface (an indicator of the wettability) can be estimated from van der Waals and double layer forces. According to Chiquet [14], the change in double-layer forces is due to a reduction in the pH of water phase, which is a consequence of CO_2 dissolution into water. This makes the water film unstable, so altering the wettability of the system. Our study has not been performed with the planar substrates, however being all silica surfaces a comparison should be possible. At the pore scale we do not see any significant alteration in the wettability while increasing the pressure of the system. We observe similar shape of the interfaces, as well as the existence of thin water films around the solid surface for gaseous (low density) as well as for liquid or supercritical (high density) CO_2. This indicates that for all these experiments the system could be considered as strongly water-wet. For all our experiments, none of the two phases was observed as a dispersed phase in the porous media. Both phases were well connected. One factor that could explain the differences of our results compared with those of Chiquet, is fluid phase equilibriums, which have a significant impact on interfacial properties.

3.4.2 Intermediate-Wet

In the intermediate-wet conditions the fluid distribution depends strongly on Pressure and Temperature conditions. At low pressure and low temperature, $P = 60$ bars and $T = 25$ °C, some interfaces show a strong water-wet behavior (analogous
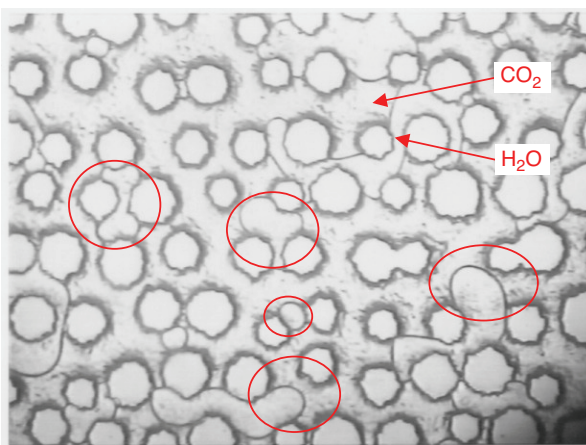

Figure 12

OW micromodel. $P = 100$ bars, $T = 23°C$.

to that showed in *Fig. 10*). Other interfaces have a contact angle close to 90° which corresponds to an intermediate-wet behavior. These differences could be explained from a non-uniform efficiency of the wettability alteration process. At this scale no water or CO_2 film has been observed. In some areas, the water phase does not seem to be connected, however it is tough to say if it is a dispersed phase because water saturation is still important.

Figure 15 shows a CO_2 flooding at $P = 100$ bars and $T = 60°C$.

Figure 11 shows a CO_2 flooding at $P = 100$ bars and $T = 25°C$. Under these conditions, most of the interfaces show that the wetting fluid is the CO_2 instead of the water. The water saturation is very low and it is clear that the water phase is present only as a dispersed phase. This wetting

behavior of CO_2 was also observed at the same pressure but a higher temperature ($P = 100$ bars and $T = 60°C$). At this temperature we have not observed the water as a dispersed phase as observed at $T = 25 °C$. This wetting behavior of the CO_2 could be explained from the solubility of CO_2 into water, which leads to a lower pH value of the aqueous phase. This affects negatively the stability of any water film present on the solid surface [13]. Chiquet *et al*. [14] have shown this effect by modeling experimental contact angles, using the DLVO theory. This CO_2 behavior should be stronger for an altered surface because of a lower affinity to water. Nevertheless, considering all the assumptions, this modeling should not be seen as predictive. As has been showed by Chang *et al*. [39] the solubility is considerably higher for low temperatures. This could explain the difference in wettability and distribution of the phases between our results at 100 bars and temperatures of 25 °C and 60°C

3.4.3 Oil-Wet

Observations for the oil wet micromodels are analogous to those for the intermediate wet as shown in Figure 12. The reason why there is not a stronger CO_2 wettability for the oil-wet micromodel, is probably related to a low efficiency of the treatment (silanization).

Core Experiments – Rock and Fluid Properties

To investigate the influence of wettability on CO_2/brine displacement, parallel to the pore-scale micromodel experiments, coreflood displacements were conducted. All the experiments were performed on a limestone sample. It was selected for its good level of homogeneity at the core scale. This is highly important when results of core flooding data, conducted at different conditions, have to be compared. The main properties of this sample are gathered in Table 4. A mercury porosimetry curve obtained on an end-cut of the sample and the NMR T2 response of the sample indicated that the pore distribution exhibited a mono-modal behavior. An initial P_c curve was also estimated from the mercury porosimetry curve, using the Leverett function. An immiscible gas/water k_r curve was obtained by the UnSteady-State method, while performing an history match of the experimental data with a 1-D numerical simulator. A Pore Network Model (PNM) approach [40] was also applied to double check that these k_r and P_c curves were representative of the rock-type of the sample.

Table 5 presents the injecting fluid, N_2 or CO_2, and the operating conditions of each coreflood experiment. Wettability indices were deduced from P_c curves obtained by centrifuge. The indices were calculated using the USBM method. As seen in Table 5, in one case the sample is strongly water-wet and in the other cases it is intermediate-wet. The intermediate wettability was obtained while aging the sample in crude oil at 60°C during one month.

The used brine was composed of 5 g/L NaCl.

TABLE 4

Properties of the rock sample

	Sample at WW state	Sample at IW state
Permeability (mD)	1.0	4.0
Porosity (%)	23.6	23.6
Length (cm)	11.8	11.8
Diameter (cm)	4.93	4.93
Pore volume (cm³)	54.74	54.74

TABLE 5

Operating conditions of the experiments

Inj. fluid	Pressure (bars)	Temp (°C)	Q inj. (cm³/h)	Wet. index	Kabs (mD)
CO_2	100	60	5-25-100	0.63	4.0
N_2	100	60	5-25-100	-0.01	1.0
CO_2	100	60	5-25-100	-0.01	1.0

Coreflood Experiments

In order to obtain P_c data at different wettability states CO_2 and N_2 multi-rate injections were performed in the selected sample. These UnSteady-State coreflood were performed in drainage, at reservoir conditions *(Tab. 5)*. The local saturation of both phases was recorded continuously. For the interpretation of the experiments, the heterogeneous approach was applied. More information about the heterogeneous approach can be founded elsewhere [41].

Results and Discussion

Figures 13, 14 and 15 present the P_c curves obtained for each core flooding. Figure 13 shows that the experimental P_c data match the P_c curve derived from the mercury porosimetry curve (using the Leverett function for a contact angle of 0°), especially for the low and medium flow rates. Hence, at reservoir conditions, the obtained P_c data indicates a strongly water-wet system for an initially water-wet sample. In Figure 14, the same behavior can be observed, but in this case, with an intermediate-wet sample. Therefore, according to the P_c, N_2 does not wet the rock surface, even if the rock has an intermediate wettability. The case of a CO_2 injection in the intermediate-wet sample *(Fig. 15)* is different: it is necessary to use a contact angle of 55°, in the Leverett function, to match the experimental values. This indicates that for an intermediate-wet sample, the CO_2 partially wets the solid surface. These data are coherent with the visual experiments presented previously in this paper. Nevertheless, it is interesting to notice that at the macro scale (sample scale, *i.e.* Darcy scale), the wetting behavior of the CO_2 seems to be less important compared to the one observed at the pore scale (micromodels). A similar trend can be identified while comparing the contact angle evolution reported by Chiquet *et al*.
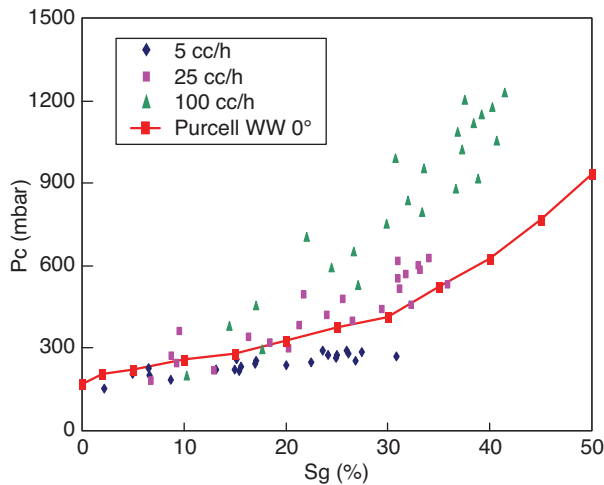
Figure 13

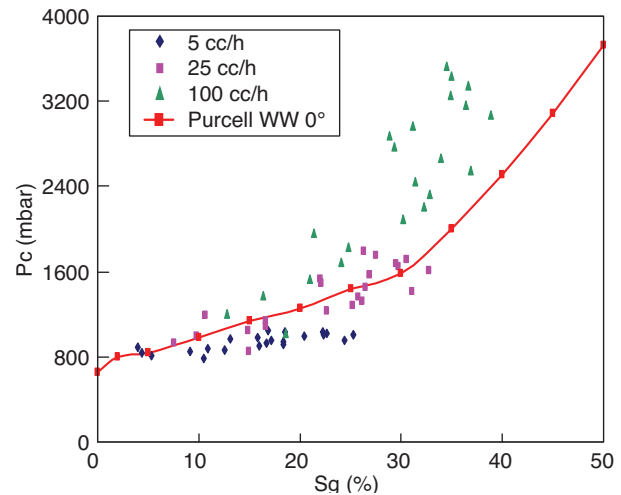P_c curve. CO_2 injection, water-wet sample.

Figure 14

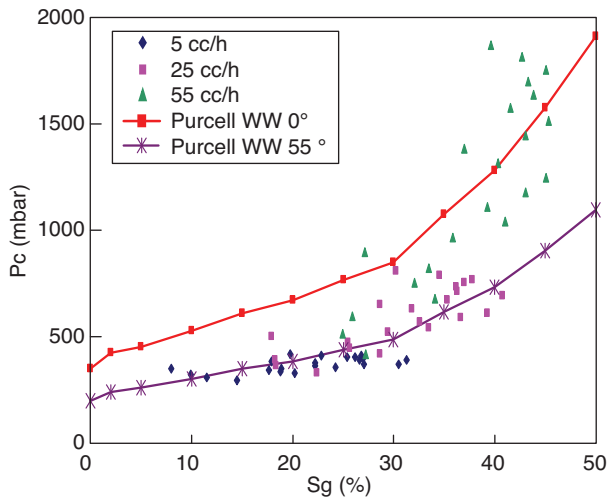P_c curve. N_2 injection, IW sample.

Figure 15

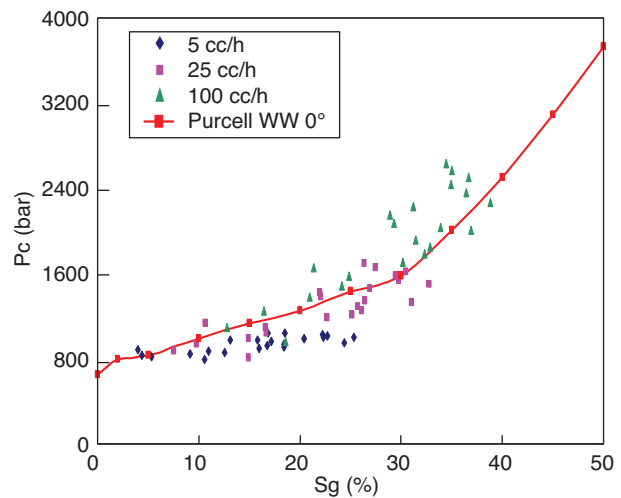P_c curve. CO_2 injection, IW sample.

Figure 16

P_c curve. N_2 injection, IW sample after extrapolation of production data.

[13] with the results obtained in this study at the pore scale *(see Sect. 2)*. The contact angle measurements suggest a change in wettability of the systems while increasing pressure. At a larger scale, the pore scale, some changes were observed in the distribution of the phases and in the shape of the interfaces, but the media seemed to keep water wettability while increasing pressure.

In Figures 13 to 15, at the highest rate, a deviation exists between the values obtained at reservoir conditions and the curve derived from the Purcell data. In these experiments, the injected CO_2 or N_2 is limited by the volume of the CO_2 or N_2 cell (1 liter). It means that for a rate of 100 cm³/h, there is always the risk to have to stop the experiment

before the system has reached a complete stabilization, both in the cumulative brine production and in the pressure drop. In order to verify the hypothesis that this deviation is, at least partly, due to a stabilization problem, the pressure drop was extrapolated to longer times, using an exponential law. This was done for the N_2 injection experiments because of the availability of more data points at the higher rate, compared to the experiments with CO_2. Figure 16 (to be compared to *Fig. 14*) shows a good agreement between the Purcell curve, the experimental (5 cc/h and 25 cc/h) and extrapolated (100 cc/h) data. The deviation was effectively due to a stabilization issue.
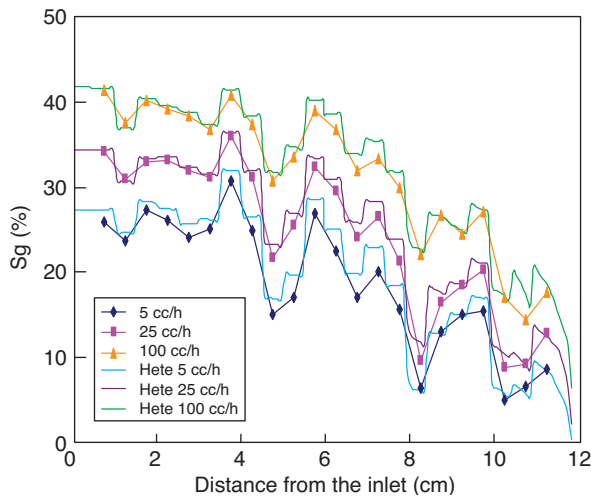
Figure 17

History matching of the saturation profiles with local P_c data. CO$_2$ injection in a WW sample.
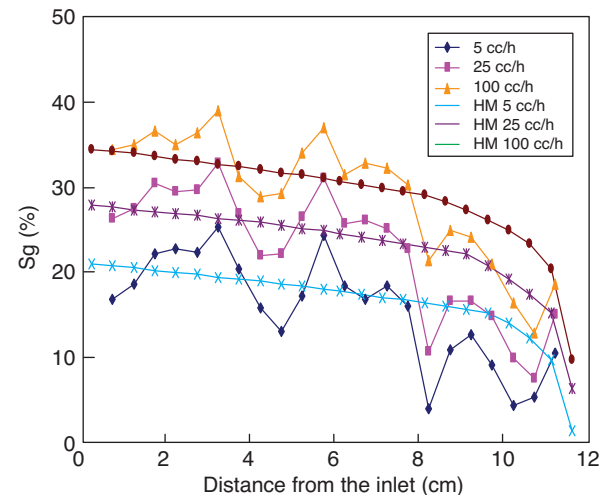

Figure 18

Initial history matching (homogeneous model) of the saturation profiles. CO$_2$ injection in a WW sample.
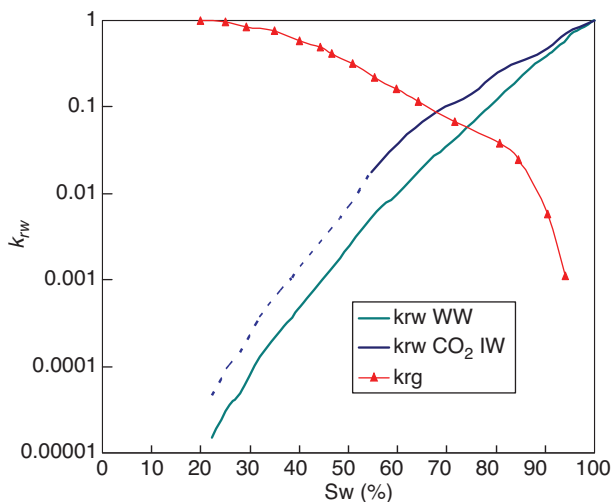

Figure 19

k_r curves for the CO$_2$ core flooding experiments.

For each coreflood, the $P_c(S_g)$ values presented in Figures 1 to 16 were introduced into the simulation model as local P_c curves, for different sections of the sample, in order to match the heterogeneities observed in the saturation profiles. For the CO$_2$ injection in a WW sample, Figure 17 shows the good agreement between the measured saturation profiles and the profiles obtained by history match. Figure 17 must be compared to Figure 18 in order to appreciate the degree of improvement in this history matching. Only one iteration was needed to obtain these results. This demonstrates the ability of the pressure data to account for the heterogeneities.

Possible implications of a wetting CO$_2$ in geological storage

According to the previous pore and core scale observations the CO$_2$ can wet the surface if this surface is not strongly water-wet. In terms of capillary-sealing efficiency, the effect of a wetting CO$_2$ at reservoir conditions is detrimental to CO$_2$ underground storage. Actually, from Equation (3), this implies to lower the threshold value of the capillary pressure. Hence a lower amount of CO$_2$ could be stored in a given intermediate-wet reservoir, compared to a strongly water-wet one, because of an earlier breakthrough in the caprock.

In terms of CO$_2$ displacement efficiency, the performed experiments showed a water cumulative production 20% higher for the intermediate-wet scenario compared to the water-wet scenario. Therefore, it is possible to reach higher CO$_2$ saturations in the reservoir if CO$_2$ partially wets the rock. This is coherent with the micromodel observations of a water dispersed phase. Figure 19 shows the k_r data obtained for each CO$_2$ core flooding experiment. A higher k_{rw} was obtained for the CO$_2$ injection in the case of the intermediate-wet sample. Therefore, the higher displacement efficiency cannot only be attributed to a lower P_c, but also to a higher mobility of the water phase. k_{rg} curves have also be estimated, but no significant difference has been observed between the WW and IW cases.

The increase in the displacement efficiency could be considered as an advantage for the CO$_2$ storage in oil depleted reservoirs presenting an intermediate wettability. But an intermediate wettability could be hardly found in an aquifer.

CONCLUSIONS

The first part of this paper presents a complete set of experimental values of brine-CO_2 interfacial tension, at pressure and temperature conditions that can be considered as representative of those of a CO_2 storage operation. The objective of this systematic study was to enable estimation of the brine-CO_2 interfacial tension at reservoir conditions, and to evaluate the evolution of this physical property with different reservoir parameters: temperature, pressure and salinity. A correlation has been proposed in order to model IFT values with a low deviation from experimental data.

The second part of this paper presents an original experimental study of the impact of wettability on CO_2 storage. Experiments were carried out under representative thermodynamic conditions, at two different physical scales:
– the pore scale by means of a qualitative study in glass micromodels;
– the core scale by means of a quantitative study in a carbonate sample.

Only the drainage process was investigated in this study. In a limestone rock under reservoir conditions, the CO_2 partially wets the surface when the surface is IW or OW. This wetting behavior of the CO_2 induces a lower capillary pressure and a higher mobility of the brine phase. The observations at the pore scale in glass micromodels are consistent with the results obtained at the core scale concerning the wetting behavior of the CO_2 at reservoir conditions. At the pore-scale the contact angle, the shape of the interfaces and the presence of the water phase as a dispersed phase provide clear evidences of this wettability change. Among the effects of a partial wetting of the CO_2 there is a lower capillary breakthrough pressure of the caprock, as can be deduced from Equation (1). This has negative impact on the capacity of the reservoir, hence on the amount of CO_2 that can be stored.

Future work: the imbibition process has not been evaluated. The knowledge and quantification of the k_r hysteresis between the drainage and the imbibition curves is very important to estimate the capillary trapping of CO_2 [42, 43]. This issue has been investigated by simulation [43-45]. Few experimental relative permeability determinations, specifically for that point, are available. Therefore future experimental work should be done to further investigate drainage and imbibition processes, in order to improve the estimation of the amount of CO_2 that is susceptible to be safely injected.

REFERENCES

1 International Energy Agency (2004), *Prospects for CO₂ Capture and Storage,* OECD/IEA, Paris.

2 Orr Jr F.M. (2004) Storage of Carbon Dioxide in Geologic Formations, SPE 88842, Distinguished Author Series, *J. Petrol. Technol.* September, 90-97.

3 Heuer G.J. (1957) Interfacial Tension of Water Against Hydrocarbon and Other Gases and Adsorption of Methane and Solids at Reservoir Conditions, *PhD Thesis*, The University of Texas at Austin.

4 Chun B.S., Wilkinson G.T. (1995) Interfacial Tension in High Pressure Carbon Dioxide Mixtures, *Ind. Eng. Chem. Res.* **34**, 4371-4377.

5 Harrison K. (1996) Interfacial Tension Measurements of CO₂-Polymer and CO₂-Water Systems and Formation of Water-in-CO₂ Microemulsions, *PhD Thesis*, The University of Texas at Austin.

6 Hebach A., Oberhof A., Dahmen N., Kögel A., Ederer H., Dinjus E. (2002) Interfacial Tension at elevated Pressures-Measurements and Correlations in the Water + Carbon Dioxide System, *J. Chem. Eng. Data* **47**, 1540-1546.

7 Ennis-King J., Paterson L. (2003) Role of Convective Mixing in the Long Term Storage of Carbon Dioxide in Deep Saline Formations, paper SPE 84344, *SPE Annual Technical Conference and Exhibition*, Denver, October 5-8.

8 Da Rocha S.R.P., Johnston K.P., Westacott R.E., Rossky P.J. (2001) Molecular Structure of the Water-Supercritical CO₂ Interface, *J. Phys. Chem. B* **105**, 1292-12104.

9 Kuznetsova T., Kvamme B. (2002) Thermodynamic Properties and Interfacial Tensions of a Model Water-Carbon Dioxide, *J. Phys. Chem.* **4**, 937-941.

10 Yan W., Zhao G.-Y., Chen G.-J., Guo T.-M. (2001) Interfacial Tension of (Methane + Nitrogen) + Water and (Carbon Dioxide + Nitrogen) + Water Systems, *J. Chem. Eng. Data* **46**, 1544-1548.

11 Zuo Y.-X., Stenby E. (1998) Calculation of Interfacial Tensions of Hydrocarbon-Water Systems Under Reservoir Conditions, *In Situ* **22**, 157-180.

12 Yang D., Gu Y. (2004) Interfacial Interactions of Crud Oil-Brine-CO₂ Systems under Reservoir Conditions, SPE 90198, *SPE Annual Technical Conference and Exhibition*, Houston, Sept. 26-29.

13 Chiquet P., Broseta D., Thibeau S. (2005) Capillary Alteration of Shally Caprocks by Carbon Dioxide, SPE 94183, *14th Europec Biennial Conference*, Madrid, June 13-16.

14 Chiquet P. (2006) Mécanismes thermophysiques déterminant la sécurité du stockage géologique du CO₂, *Thèse*, Université de Pau et des Pays de l'Adour.

15 Egermann P., Banini S., Vizika O. (2004) Depressurization Under Tertiary Conditions in the Near-Wellbore Region: Experiments, Visualization and Radial Flow Simulations, *J. Petrophys.* **45**, 5, 422-432.

16 Søreide I., Whitson C.H. (1992) Peng-Robinson Predictions for Hydrocarbons, CO₂, N₂, H₂S with Pure Water and NaCl Brine, *J. Fluid Phase Éq.* **77**, 217-240.

17 Rowe A.M., Chou J.C.S. (1970) Pressure-Volume-Temperature-Concentration Relation of Aqueous NaCl Solutions, *J. Chem. Eng. Data* **15**, 61-66.

18 King M.B., Mubarak A., Kim J.D., Bott T.R. (1992) The Mutual Solubilities of Water with Supercritical and Liquid Carbon Dioxide, *J. Supercrit. Fluid.* **5**, 296-302.

19 Lahooti S., del Río O.I., Cheng P., Newmann A.W. (1996) *Applied Surface and Thermodynamics,* Vol. 1, Neumann A.W., Spelt J.K. (eds), Marcel Dekker, New York.

20 Chalbaud C., Robin M., Lombard J.-M., Egermann P., Bertin H. (2009) Interfacial Tension Measurements and Wettability Evaluation for Geological CO₂ Storage, *Adv. Water Resour.* **32**, 1, 1-109.

21 Massoudi R., King Jr. (1975) Effect of Pressure on the Surface Tension of Aqueous Solutions. Adsorption of Hydrocarbon Gases, Carbon Dioxide, and Nitrous Oxide on Aqueous Solutions of Sodium Chloride and Tetra-n-butylammonium Bromide at 25°C, *J. Phys. Chem.* **79**, 16, 1670-1675.

22 Wiebe R. (1941) The Binary System Carbon Dioxide-Water Under Pressure, *Chem. Rev.* **29**, 475-489.

23 Malinin S.D., Savelyeva N.I. (1972) The Solubility of CO₂ in NaCl and CaCl₂ Solutions at 25, 50 and 75°C under Elevated CO₂ Pressures, *Geochem. Int.* **9**, 1, 410.

24 Malinin S.D., Kurovskaya N.A. (1975) Solubility of CO₂ in Chloride Solutions at Elevated Temperatures and CO₂ Pressures, *Geochem. Int.* **2**, 2, 199.

25 Argaud M.J. (1992) Predicting the Interfacial Tension of Brine/Gas (or Condensate) systems, *European Core Analysis Symposium*, Paris, September 14-16.

26 Aveyard R., Saleem S.M. (1975) Interfacial Tension at Alkane-Aqueous Electrolyte Interfaces, *J.C.S. Faraday* **73**, 1613-1617.

27 Johansson K., Eriksson J.C. (1974) γ and dγ/dT Measurements on Aqueous Solutions of 1.1 Electrolytes, *J. Colloid. Interf. Sci.* **49**, 3, 469-480.

28 Chiquet P., Daridon J.-L., Broseta D., Thibeau S. (2007) CO₂/Water Interfacial Tension under the Pressure and Temperature Conditions of CO₂ Geological Storage, *Energ. Convers. Manage.* **48**, 3, 736-744.

29 Washburn E.D. (1928) *International Critical Tables*, McGraw-Hill, NY, Vol. 4.

30 Egermann P., Chalbaud C., Duquerroix J.-P., Le Gallo Y. (2006) An Integrated Approach to Parameterize Reservoir Models for CO₂ Injection in Aquifers, SPE 102308, *SPE Annual Technical Conference and Exhibition*, San Antonio, September 24-27.

31 Firoozabadi A., Ramey H.J. (1988) Surface Tension of Water-Hydrocarbon Systems at Reservoir Conditions, *J. Can. Petrol. Technol.* **27**, 3, 30-39.

32 Reno G.J., Katz D.L. (1943) Surface Tension of n-Heptane and n-Butane Containing Dissolved Nitrogen, *Ind. Eng. Chem.* **35**, 10, 1091-1093.

33 McLeod D.B. (1923) On a Relation Between Surface Tension and Density, *Trans. Farad. Soc.* **19**, 38-43.

34 Fowler R.H. (1937) A Tentative Statistical Theory of McLeod's Equation for Surface Tension and the Parachor, *Proc. R. Soc. Lond.* A, 229-246.

35 Schechter D.S., Guo B. (1995) Parachors Based on Modern Physics and Theirs Uses in IFT Prediction of Reservoir Fluids, SPE 30785, *SPE Annual Technical Conference and Exhibition*, Dallas, October. 22-25.

36 Chalbaud C. (2007) Propriétés Interfaciales du CO₂. Application aux Écoulements en Pression et Température, *Thèse*, École Nationale des Arts et Métiers.

37 Chalbaud C., Robin M., Bekri S., Egermann P., Bertin H. (2007) Wettability Impact on CO₂ Storage in Aquifers: Visualization and Quantification Using Micromodels, Pore Network Model and Reservoir Simulation, *SCA International Symposium*, Calgary, September 12-15.

38 Israelachvili J.N. (1991) *Intermolecular & Surface Forces*, Academic Press, 2ᵉ ed., New York.

39 Chang Y.-B., Coats B.K., Nolen J.S. (1998) A Compositional Model for CO₂ Floods Including CO₂ Solubility into Water, SPE 35164, *SPE Reservoir Evaluation and Engineering*, April.

40 Békri S., Laroche C., Vizika O. (2005) Pore Network Models to Calculate Transport and Electrical Properties of Single and Dual Porosity Rocks, *Society of Core Analysis Symposium*, Toronto, August, pp. 21-25.

41 Egermann P., Lombard J.-M., Fichen C., Rosenberg E., Tachet E., Lenormand R. (2005) A New Experimental Method to Determine Interval of Confidence for Capillary Pressure and Relative-Permeability Curves, SPE 96896, *SPE Annual Technical Conference and Exhibition*, Dallas, October 9-12.

42 Imbus S., Orr F.M., Kuurskraa V.A., Kheshgi H., Bennaceur K., Gupta N., Rigg A., Hovorka S., Myer L., Benson S. (2006) Critical Issues in Capture and Storage: Findings of the SPE Advanced Technology Workshop (ATW) on Carbon Sequestration, SPE 102968, *SPE Annual Technical Conference and Exhibition*, San Antonio, September 24-27.

43 Spiteri E.J., Juanes R., Blunt M.J., Orr F.M. (2005) Relative Permeability Hysteresis: Trapping Models and Application to Geological CO₂ Sequestration, SPE 96448, *SPE Annual Technical Conference and Exhibition*, Dallas, October 9-12.

44 Juanes R., Spiteri E.J., Orr F.M., Blunt M.J. (2006) Impact of Relative Permeability Hysteresis on Geological CO₂ Storage, *Water Resour. Res.* **42**, 12.

45 Flett M., Gurton R., Taggart I. (2004) The Function of Gas-Water Relative Permeability Hysteresis in the Sequestration of Carbon Dioxide in Saline Formations, SPE 88485, *SPE Asia Pacific Oil and Gas Conference and Exhibition*, Perth, October 18-20.